XLVI CILAMCE
VITÓRIA - ES - BRAZIL - 2025
XLVI IBERO-LATIN AMERICAN CONGRESS ON COMPUTATIONAL METHODS IN ENGENEERING

Alternative numerical model for vehicle–bridge interaction based on the positional finite element method

Geovana Viviani de Araujo[1], Tiago Morkis Siqueira[1]

[1]*Department of Civil Engineering, Federal University of Santa Catarina (UFSC)*
João Pio Duarte da Silva -205, 88037-000, Florianópolis, SC, Brazil
geovana.viviani@grad.ufsc.br, tiago.morkis@ufsc.br

Abstract. Vehicle-Bridge Interaction (VBI) describes the coupled dynamic response generated when a vehicle crosses a bridge, where both systems influence each other, producing an integrated dynamic behavior. VBI models typically combine analytical vehicle dynamics with numerical bridge representations. Bridges are often discretized with finite element models, commonly using beam elements. Vehicles are usually assumed as mass-spring-damper systems representing the truck, trailer, and axles. This work employs an alternative vehicle model representation, which is mechanically equivalent to the conventional systems, by properly placing plane frame finite elements in the model. Nonlinear geometric effects from large vehicle displacements relative to the bridge are incorporated via a positional finite element formulation. A modified Kelvin-Voigt viscoelastic model is employed for the materials and adjusted for the spring-dampers of the vehicle model. Lagrange multipliers enforce coupling between vehicle and bridge elements using sliding connections. Road surface roughness along the vehicle path is also included. The simulated dynamic responses are compared with the literature showing the accuracy of the proposed modelling in representing the VBI problem.

Keywords: numerical simulation; structures; nonlinear analysis; dynamics.

1 Introduction

Safety and performance of highway bridges are topics of great relevance in civil engineering, especially considering the constant increase in the volume and weight of vehicle traffic [1]. In this context, Vehicle-Bridge Interaction (VBI) is a complex dynamic phenomenon where the responses of the vehicle and bridge are intrinsically coupled. The passage of vehicles mobilizes the dynamic response of the structure, whose effects can be significant, resulting in vibrations and, at times, stresses and deformations greater than those expected based solely on static analyses.

The need for in-depth studies on VBI is current, especially considering the particularities of bridges and traffic in Brazil [2], as well as technological advancements in fleets, such as the growing adoption of electric vehicles with considerable weight. Furthermore, there is great interest in numerical models representing VBI for use such as in Structural Health Monitoring systems [3, 4] to assess structural anomalies, fatigue damage, and long-term deterioration for instance.

VBI models typically combine analytical vehicle dynamics with numerical bridge representations [5–10]. Bridges are often discretized with finite element models, commonly using beam elements, whereas vehicles are usually assumed as mass-spring-damper systems representing the truck, trailer, and axles.

Differently from the usual approach, in this study, the vehicle is modeled by properly placed plane frame finite elements, replicating the mechanical behavior of those mass-spring-damper models. This alternative approach provides general modeling of vehicles with different geometries (number of axles, arrangement of masses, springs and dampers) without the need to develop new mass-spring-damper equations of motion for such modifications.

The sliding coupling between vehicle and its path (bridge and ground), including pavement roughness, is achieved using Lagrange multipliers to enforce contact. This is facilitated due to the positional approach of the

finite element method [11, 12] that uses positions as the element's degrees of freedom (DOF), instead of nodal displacements. Being a total Lagrangian formulation, finite deformation due to vehicle displacements relative to the bridge is naturally incorporated in the formulation.

A modified Kelvin-Voigt viscoelastic material [11] is employed, particularly to represent the vehicle springs and dampers. This model is an extension of the Saint-Venant-Kirchhoff hyperelastic material to include internal material viscosity in a large deformation context.

The next section briefly presents the nonlinear finite element formulation employed. The alternative vehicle modelling proposed is detailed in the following sections. Results are compared with the literature to evaluate the suitability and representativeness of the coupled dynamic responses obtained using the proposed methodology.

2 Nonlinear Finite Element Formulation

The equations of motion for the discretized finite element system comprising large displacements in a total Lagrangian description, viscoelastic material model and constraints due to sliding connections are obtained from a variational principle, as developed in detail in Siqueira and Coda [11, 12], and result in the compact expression

$$\vec{F}^{\text{int}} - \vec{F} + \mathbf{M}\cdot\ddot{\vec{Y}} + \mathbf{D}\cdot\dot{\vec{Y}} + \vec{F}^{\text{con}} = \vec{0} \tag{1}$$

where $\vec{Y}$ is the vector gathering the current value of all system degrees of freedom (from the frame elements and from the sliding connections) and the over-dot represents time derivative. $\mathbf{M}$ and $\mathbf{D}$ are the system mass and velocity-proportional external damping constant matrices. $\vec{F}$ is the vector of external forces.

The vector $\vec{F}^{\text{int}}$ in Eq. (1) represents the finite elements internal force vector due to the large deformation of the solid and its material response. For a finite element of initial volume V_0 it can be written as

$$\vec{F}^{\text{int}} = \int_{V_0} \mathbf{S} : \frac{\partial \mathbf{E}}{\partial \vec{Y}}\, dV_0 \tag{2}$$

being $\mathbf{E}$ the Green strain measure and $\mathbf{S}$ the second Piola-Kichhoff stress, which, for the employed modified Kelvin-Voigt material is the total stress acting on a point, written as the sum of elastic and viscous parts as

$$\mathbf{S} = \mathbf{C} : \mathbf{E} + \mathbf{N} : \dot{\mathbf{E}} = \begin{bmatrix} \mathrm{E}\,E_{11} & 2\mathrm{G}\,E_{12} \\ 2\mathrm{G}\,E_{12} & \mathrm{E}\,E_{22} \end{bmatrix} + \begin{bmatrix} \vartheta_h \mathrm{E}\,\dot{E}_{11} & 2\vartheta_d \mathrm{G}\,\dot{E}_{12} \\ 2\vartheta_d \mathrm{G}\,\dot{E}_{12} & \vartheta_h \mathrm{E}\,\dot{E}_{22} \end{bmatrix} \tag{3}$$

where E and G represent, in small strains, the Young and shear elastic modulus, ϑ_h and ϑ_d are viscous coefficients governing the hydrostatic and deviatoric parts of the viscous stress term (particularly the time rate of change of the strain components).

The derivative of the Green strain in Eq. (2) depends on the plane frame kinematics and its nodal parametrization: a node α current position (coordinates) Y_i^{α} $(i = 1, 2)$ and cross section angle θ_{α}, Fig. 1 a).

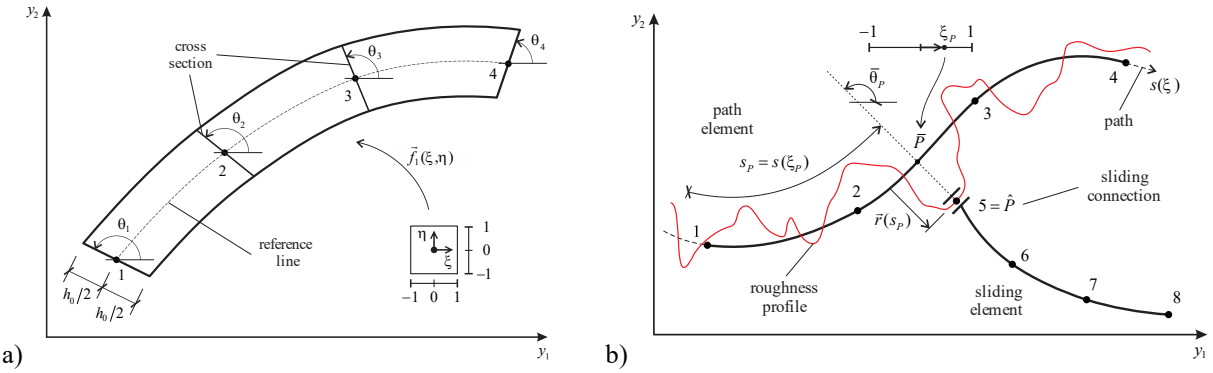


Fig. 1. Plane finite element: a) mapping $\vec{f}_1$ from a non-dimensional space (ξ, η) to the current configuration of a four-node (cubic) plane frame finite element and b) sliding connection between a sliding element node and the reference line of a path element over an arbitrary roughness profile

Still in Eq. (1), $\vec{F}^{\text{con}}$ represents the restriction forces introduced in the finite element system arriving from the constraint equations $\vec{c}$. It can be organized as a vector where the first component contributes on the nodal parameters' equations and the second one on the multipliers $\vec{\lambda}$ as

$$\vec{F}^{\text{con}} = \begin{Bmatrix} \nabla\vec{c}\cdot\vec{\lambda} \\ \vec{c} \end{Bmatrix} \tag{4}$$

The constraint equation included to represent sliding connections between frame elements (used to connect vehicle along its path) restricts a sliding node current position $\hat{Y}_i^P$ to be in contact to the current position of a path, Fig 1 b). The path is defined by a sequence of reference lines of path frame elements, that may be in contact with the sliding node, and by an arbitrary roughness profile $\vec{r}(s_P)$. The profile is measured from a reference point with the curvilinear variable to the current contact point s_P (a new unknown obatained during the solution procedure). For the present study, the constraint equation writes

$$c_i = \hat{Y}_i^P - \phi_\ell(\xi_P)\overline{Y}_i^\ell - r_i(s_P)(1-\delta_{(i)3}) = 0_i \qquad (i=1,2) \tag{5}$$

where δ_{ij} is the Kronecker delta, $\overline{Y}_i^\ell$ are the current positions of the path element nodes ℓ and $\phi_\ell(\xi_P)$ the finite element shape functions evaluated at the current contact point. $\xi_P = \xi_P(s_P)$ represents the contact point in the non-dimensional space.

As shown in this brief discussion, the terms in Eq. (1) depend on the current values of the parameters, thus rendering the equation of motion nonlinear. Its solution is performed using the Newton-Raphson method along with the generalized-α time integration scheme [13]. The detailed procedure is described in [11, 12], also including the discussion on identifying the contact point.

3 Alternative VBI Modelling Strategy

To verify the proposed mechanically equivalent alternative vehicle models, simulations using the same bridge and vehicles as described by Ding et al. [14], based upon the experimental works of Green and Cebon [15], were performed.

Vehicles in Ding et al. [14], are modelled by simplified masses-springs-dampers systems, the bridge dynamical response is considered by modal superposition and interaction is done directly by coupling the dynamic axle force from the vehicle to the bridge. Also, the reference employed the Runge-Kutta method for the solution of the equations of motion.

Two vehicle models, a quarter and half car, were evaluated for different traveling speeds on the same bridge. As the roughness profile usually employed to consider vibrations due to pavement imperfection is randomly generated, an initial analysis is performed without pavement roughness to evaluate a deterministic response of the system.

3.1 Mass-spring-damper vehicle models

A quarter-car model, Fig. 2 a), is a 2-DOF model, and represents the vehicle as a single axle. It consists of two spring-damper systems and includes two masses m_1 and m_2. The springs stiffness is represented by k_t and k_s for the tire and suspension, respectively, and the dampers coefficient is c_t and c_s for the tire and suspension. This very simple model is suitable for preliminary analyses and early-stage design evaluations.

The half-car is a 4-DOF model, Fig. 2 b), where an additional axle is considered in order to support a suspended rigid body representing the vehicle with mass M_V and inertia I_V. The center of the rigid body is defined by the axle spacing S and the position parameters a_1 and a_2. This modeling approach allows consideration of more complex dynamic effects, including mass distribution. Furthermore, dividing the vehicle into more axes provides higher fidelity simulation of relative movements between vehicle components and the bridge structure.

The VBI data described in Ding et al. [14] were adopted for the simulations performed.

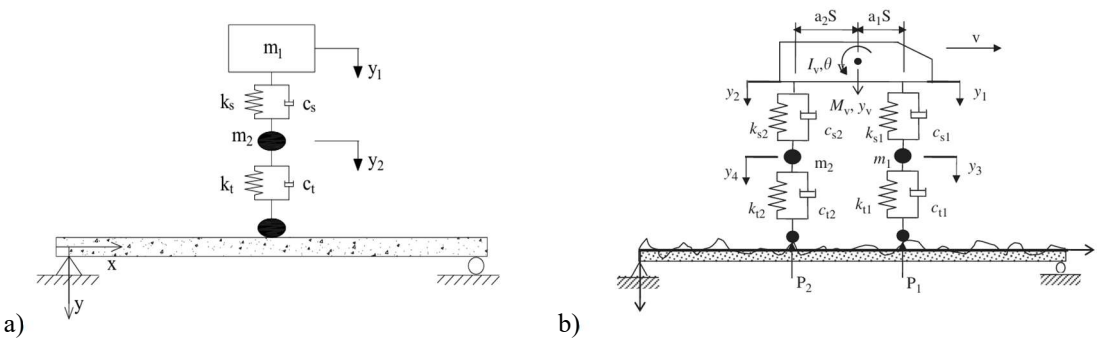


Fig. 2. Simplified vehicle models: a) a quarter-car and b) half-car model. Source: Adapted from Ding et al. [14]

3.2 Proposed equivalent finite element vehicle models

The quarter-car (1-axle vehicle, Fig. 3 a), and half-car (2-axle vehicle, Fig. 3 b), models were discretized using beam elements for the dynamic VBI analysis. The quarter-car model consists of two elements, representing system suspension, tire and the lumped masses. The half-car model additionally includes a rear axle and a horizontal bar representing the rigid vehicle chassis with concentrated mass and rotational inertia.

Suspensions and tires are modeled as viscoelastic materials. Masses are lumped at the specified nodes, and sliding joints enable longitudinal movement of the tires over the bridge. Spherical joints connect the suspensions to the chassis, allowing free rotation without the transmission of bending moments as in the reference models.

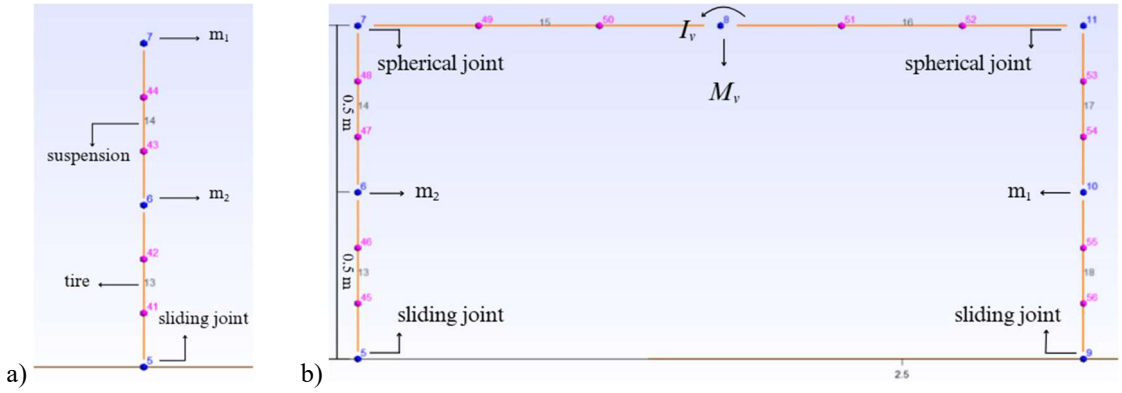


Fig. 3. Proposed vehicle meshes (cubic 4-node elements): a) a quarter-car and b) half-car model.

Geometrical properties and parameters were defined to ensure equivalence with the mass-spring-damper model from the reference [14]. However, as the frame element Kelvin-Voigt material model uses different parameters than the spring-damper, an equivalence needs to be made to use the usual stiffness k and damping c data from [14]. As the vehicle horizontal motion will be imposed in all its nodes and only vertical motion occurs, the finite elements acting as spring-dampers, either for the tire or suspension, are in a uniaxial state of stress. Recalling Eq. (3), only the element axial stress S_{11} is non null. Assuming the cross-section area variation during deformation is small and multiplying the stress component by the bar initial area A_0, results the centered force acting at the bar $F = A_0 \mathrm{E}\, E_{11} + A_0 \vartheta_h \mathrm{E}\, \dot{E}_{11}$.

The force in the usual spring-damper is obtained by $F = k\,u + c\,\dot{u}$, being u the elongation of the spring-damper system. Assuming a regimen of small strains where $E_{11} \cong u / L_0$, being L_0 the initial length of the finite element discretized bar, substituting and comparing with the force obtained by the Kelvin-Voigt material model results the relations used to convert parameters: $\mathrm{E} = kL_0 / A_0$ and $\vartheta_h = cL_0 / (EA_0)$. As no shearing occurs in the element the deviatoric viscosity parameter ϑ_d is assumed null.

Table 1. Frame element vehicle model properties.

Component	E (Pa)	G (Pa)	ϑ_h (s^{-1})	A_0 (m^2)	L_0 (m)
A quarter-car - tire	3.6×10^9	1.8×10^9	2.0×10^{-3}	0.01	0.5
A quarter-car - suspension	0.9×10^9	0.45×10^9	8.0×10^{-3}	0.01	0.5
Half-car - tire	1.8×10^9	0.9×10^9	2.0×10^{-3}	0.01	0.5
Half-car - suspension	0.45×10^9	0.225×10^9	8.0×10^{-3}	0.01	0.5
Half-car - chassis	3.0×10^{13}	1.5×10^{13}	0.0	0.01	2.0

3.3 Bridge model and vehicle interaction

The adopted bridge model follows Ding et al. [14] and consists of a simply supported beam spanning 40 meters. The overall vehicle path, including bridge and ground, extends 120 meters, with 40-meter ground segments at each end modeled with a single cubic frame elements each and fully constrained degrees of freedom to represent rigid supports. Mesh generation was done using Gmsh [16].

The ground addition ensures proper modeling of the vehicle's motion (which requires a path before entering the bridge) and allows for the evaluation of a stationary dynamic vehicle response when reaching the bridge by starting the vehicle position distant from the bridge end. This is important in cases where surface roughness is considered. Conversely, when the ground is modeled as a perfectly smooth surface, no vehicle vibrations are expected before reaching the beam, since no external excitation is present, and the vehicle initial position could be at the bridge end.

The road surface roughness plays an important role in the dynamic responses of the vehicle-bridge interaction. The roughness profile is adopted following Oliva et al. [6] using ISO-8608 [17] road classification. Also, a rigid tread band model [18] with radius of 0.50 m is adopted to represent adequately the tire contact.

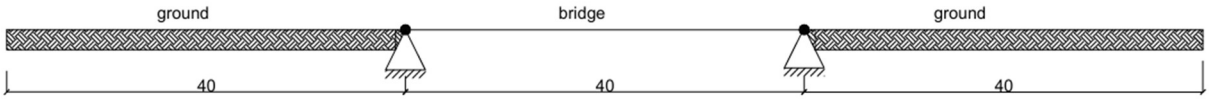


Fig. 4. Mesh model including bridge and surrounding ground segments (distance in meters).

The bridge span itself was discretized into 10 finite elements, also using cubic elements, resulting in a total of 31 nodes along the entire model. Spherical joints were employed at the ends of the bridge to enforce simply supported boundary conditions, allowing free rotation without moment transfer to the ground elements.

The properties of the bridge from the reference [14] were made equivalent by employing: E = 30.0 GPa; G = 15.0 GPa; rectangular cross-section with height 1.6198 m and width 12.0 m; and mass density 617.4 kg/m³.

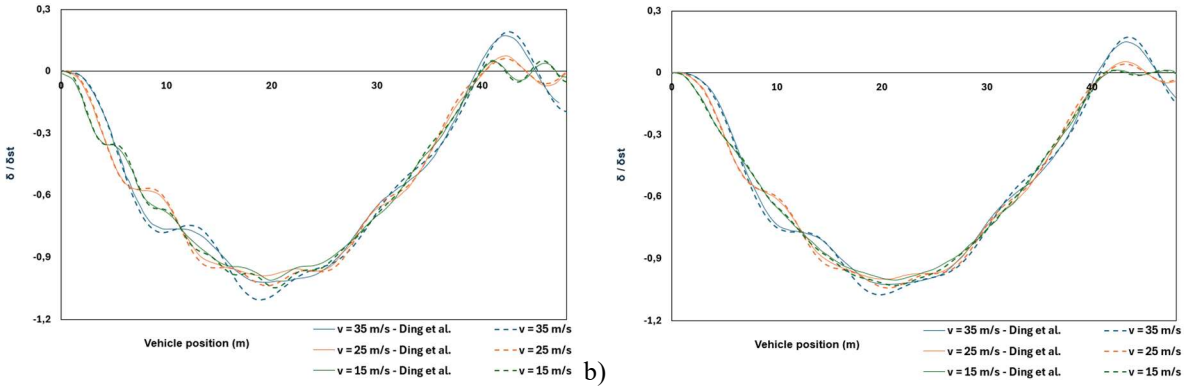
Although the bridge mass was included in the dynamic model, its self-weight was not considered in the simulations conducted to be in accordance with Ding et al. [14].

At the start of each simulation, before the dynamical simulation, 10 quasi-static steps were performed to allow the vehicle to reach a stationary response condition on the approach roadway, due to its self-weight and viscous dampers response, before entering the bridge.

Regarding time integration, preliminary simulations were conducted to determine an appropriate time step. The step size was iteratively calibrated until a value of 1×10^{-3} was reached, ensuring both accuracy and computational efficiency. For the generalized-α method a spectral radius $\rho_\infty = 0.90$ was adopted.

4 Results and Discussion

Fig. 6 presents the comparison of the normalized displacement δ/δ_{st} at the midpoint of the bridge regarding the vehicle's front axle position for the two vehicle models, considering vehicle speeds of 15, 25 e 35 m/s. Being δ_{st} the maximum static displacement of the beam which is 4.14 mm for the quarter-car model and 4.10 mm for the half-car model [14].



a) b)

Fig. 6. Comparative graphs: a) 1-axle vehicle and b) 2-axle vehicle.

It is observed that an increase in speed results in larger displacement amplitudes, as well as oscillatory responses. In contrast, for the speed of 15 m/s, a less oscillatory response is noted, with smaller displacements at the central point of the structure. Furthermore, the results for this condition show agreement with the reference data [14], demonstrating the suitability of the numerical model employed. Small differences in the simulated response and the reference are likely due to the different formulations employed, in particular the time marching schemes adopted.

Road roughness was considered for the half-car travelling at 15 m/s and modeled using a road class A profile from ISO 8608 [17], representing good pavement quality. Fig. 7 shows that the bridge behavior at the initial meters of the crossing is similar with or without roughness. However, as the vehicle progresses, the presence of pavement roughness induces oscillations in the response, demonstrating its significant influence on the system's dynamic behavior, which was especially important in this case due to the low stiffness of this particular bridge.

A test neglecting dynamic effects and assuming purely static distribution of load, Fig. 7 was performed. According to Cassola [19], in highway bridge design, dynamic effects are accounted for by amplifying static loads using the Dynamic Amplification Factor (DAF), also discussed in [14]. This factor is defined solely based on the bridge span length, as established by the Brazilian standard NBR 7187:2022 [20]. In this case of low vehicle speed, the static load results similar to the dynamical case without roughness. However, for the case closer to a real VBI condition, where pavement imperfections exist, even for a good quality road pavement, the static response differs greatly. This discrepancy highlights the importance of considering proper VBI dynamics and also applying the DAF in structural designs to ensure both the safety and adequate performance of bridges under moving loads.

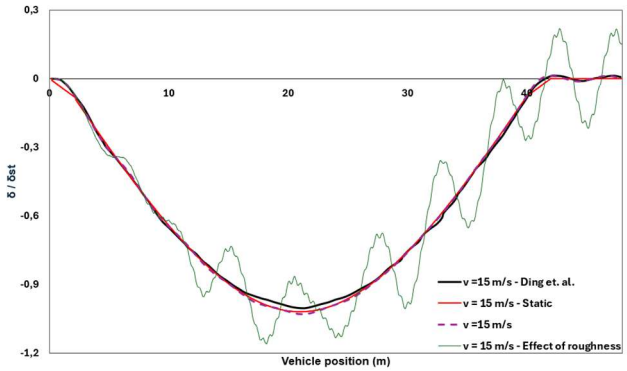


Fig. 7. 2-axle vehicle roughness and static comparison.

5 Conclusions

This work presented a mechanically equivalent alternative vehicle model representation for VBI by properly placing plane frame finite elements in the model. A total Lagrangian finite element formulation was employed to represent the nonlinear dynamical response due to the large vehicle displacements relative to the bridge. A modified Kelvin-Voigt viscoelastic model was employed for the materials and adjusted to use data from simplified springs and dampers of usual vehicle models in the proposed model. Road surface roughness along the vehicle path was also included. The simulated dynamic responses were compared with literature for two vehicle models and showed the proposed modelling accuracy in representing the VBI problem.

Authorship statement. The author hereby confirms that they are the sole liable persons responsible for the authorship of this work, and that all material that has been included as part of the present paper is either the property (and authorship) of the author, or has the permission of the owners to be included here.

References

1. Sivakumar B, Ghosn M, Moses F (2010) Adjustment of Load and Resistance Factor Design Live Load Factors Using Recent Weigh-in-Motion Data. Transp Res Rec 2200:90–97. https://doi.org/10.3141/2200-11
2. Rossigali CE, Pfeil MS, Sagrilo LVS, de Oliveira HM (2023) Load Models Representative of Brazilian Actual Traffic in Girder-Type Short-Span Highway Bridges. Appl Sci 13:1032. https://doi.org/10.3390/app13021032
3. Sarwar MZ, Cantero D (2023) Vehicle assisted bridge damage assessment using probabilistic deep learning. Measurement 206:112216. https://doi.org/10.1016/j.measurement.2022.112216
4. Sun L, Shang Z, Xia Y, et al (2020) Review of Bridge Structural Health Monitoring Aided by Big Data and Artificial Intelligence: From Condition Assessment to Damage Detection. J Struct Eng 146:04020073. https://doi.org/10.1061/(ASCE)ST.1943-541X.0002535
5. Sun Z, Zou Z (2016) Towards an efficient method of predicting vehicle-induced response of bridge. Eng Comput 33:2067–2089. https://doi.org/10.1108/EC-02-2015-0034
6. Oliva J, Goicolea JM, Antolín P, Astiz MÁ (2013) Relevance of a complete road surface description in vehicle–bridge interaction dynamics. Eng Struct 56:466–476. https://doi.org/10.1016/j.engstruct.2013.05.029
7. Wu SQ, Law SS (2011) Vehicle axle load identification on bridge deck with irregular road surface profile. Eng Struct 33:591–601. https://doi.org/10.1016/j.engstruct.2010.11.017
8. Gao Q, Zhang K, Wang T, et al (2021) Numerical investigation of the dynamic responses of steel-concrete girder bridges subjected to moving vehicular loads. Meas Control 54:465–484. https://doi.org/10.1177/0020294020981406
9. Li X-Z, Zhang L-M, Zhang J (2008) State-of-the-art review and trend of studies on coupling vibration for vehicle and highway bridge system. Gongcheng LixueEngineering Mech 25:230–240
10. González A, Covián ,Enrique, and Casero M (2023) Verifying the suitability of uncoupled numerical methods for solving vehicle-bridge interaction problems. Struct Infrastruct Eng 19:1407–1424. https://doi.org/10.1080/15732479.2022.2033276
11. Siqueira TM, Coda HB (2017) Total Lagrangian FEM formulation for nonlinear dynamics of sliding connections in viscoelastic plane structures and mechanisms. Finite Elem Anal Des 129:63–77. https://doi.org/10.1016/j.finel.2016.12.005
12. Siqueira TM, Coda HB (2023) Improved friction model applied to plane sliding connections by a large deformation FEM formulation. Lat Am J Solids Struct 20:. https://doi.org/10.1590/1679-78257321
13. Chung J, Hulbert GM (1993) A Time Integration Algorithm for Structural Dynamics With Improved Numerical Dissipation: The Generalized-α Method. J Appl Mech 60:371. https://doi.org/10.1115/1.2900803
14. Ding L, Hao H, Zhu X (2009) Evaluation of dynamic vehicle axle loads on bridges with different surface conditions. J Sound Vib 323:826–848. https://doi.org/10.1016/j.jsv.2009.01.051
15. Green MF, Cebon D (1994) Dynamic Response of Highway Bridges to Heavy Vehicle Loads: Theory and Experimental Validation. J Sound Vib 170:51–78. https://doi.org/10.1006/jsvi.1994.1046
16. Geuzaine, C., Remacle, J.-F. Gmsh (Version 4.14.0) [Computer software]. University of Liège, 2021. Available at: http://gmsh.info
17. ISO (1995) Mechanical Vibration — Road Surface Profiles — Reporting of Measured Data (ISO Standard No. 8608)
18. Captain KM, Boghani AB, Wormley DN (1979) Analytical Tire Models for Dynamic Vehicle Simulation. 8:1–32. https://doi.org/10.1080/00423117908968566
19. Cassola, S. Análise dinâmica da interação entre ponte rodoviária e veículos pesados. PhD thesis, Universidade de São Paulo, 2005
20. Associação Brasileira de Normas Técnicas. (2022). NBR 7187: Projeto de pontes de concreto – Procedimento. ABNT.